Journal of Pharmacy and Pharmacology, 2024, **XX**, 1–12
https://doi.org/10.1093/jpp/rgae122
Advance access publication 9 October 2024
Research Paper

JPP Journal of Pharmacy and Pharmacology

OXFORD

Production of mRNA lipid nanoparticles using advanced crossflow micromixing

Muattaz Hussain, Burcu Binici, Liam O'Connor, Yvonne Perrie*

Strathclyde Institute of Pharmacy and Biomedical Sciences, 161 Cathedral St., University of Strathclyde, Glasgow, G4 0RE, United Kingdom

*Corresponding author. Strathclyde Institute of Pharmacy and Biomedical Sciences, 161 Cathedral St., University of Strathclyde, Glasgow, G4 0RE, United Kingdom. E-mail: yvonne.perrie@strath.ac.uk

Abstract

Objectives: Lipid nanoparticles (LNPs) play a crucial role in RNA-based therapies, and their production is generally based on nanoprecipitation and coalescence of lipids around an RNA core. This study investigated crossflow micromixing to prepare LNPs across various mixing ratios and production speeds.

Methods: A range of LNPs were prepared using crossflow micromixing across production speeds of 10–500 ml/min, and their physico-chemical characteristics (size, polydispersity index (PDI), zeta potential, and mRNA encapsulation), *in vitro* mRNA expression and *in vitro* efficacy (protein expression and antibody and cytokine responses).

Key findings: Our results demonstrate the reproducible production of mRNA–LNPs with controlled critical quality attributes, including high mRNA encapsulation from the initial screening scale through to GMP-scale production, where the same mixing ratio can be adopted across all product speeds from 30 to 500 ml/min used.

Conclusions: We confirm the applicability of stainless-steel crossflow membrane micromixing for the entire spectrum of mRNA–LNP production, ranging from initial discovery volumes to GMP-production scale.

Keywords: mRNA; lipid nanoparticles; manufacturing; vaccines; micromixing

Introduction

Lipid nanoparticles (LNPs) are well recognized for their ability to deliver both small interfering RNA (siRNA) and longer messenger (mRNA) and self-amplifying RNA (SaRNA). LNPs protect nucleic acids from degradation and improve cellular uptake. LNPs are produced by blending a mixture of lipids dissolved in ethanol at the required lipid molar ratio with RNA dissolved typically in citrate buffer. During manufacturing, positively charged ionizable lipids electrostatically interact with negatively charged RNA, giving rise to a core. Additional lipids surround this core, and pegylated lipids contribute to forming a protective coating. Subsequent downstream processing (often employing tangential flow filtration) removes ethanol. This step also involves replacing the lower pH buffer with a physiological pH (pH 7.4) buffer, and cryoprotectants may be introduced to enhance stability when LNPs are subject to freeze–thaw processes.

Generally, LNPs are manufactured by nanoprecipitation, which is achieved by rapidly mixing an ethanolic lipid mix with the mRNA aqueous phase. While simple pipette mixing can be employed, this will result in a more heterogeneous particle size range and is not scalable—a crucial consideration for successful clinical translation. Controlled rapid mixing methods, including microfluidic or crossflow mixing [1], are commonly used for nanoprecipitation. T-mixers are widely employed in LNP manufacturing as they can comfortably handle flow rates of 60–80 ml/min and are compatible with organic solvents such as ethanol [2–4]. The mixing rate between the lipids in the solvent and the aqueous phase dictates the dilution rate of the ethanolic solution, controlling the nanoprecipitation reaction. This control is crucial for governing the solubility of the lipids and, hence, the lipid aggregation rate [5]. Therefore, by controlling the mixing, you can control the rate of polarity change and, consequently, the rate of nanoprecipitation. Thus, the ethanol–lipid to mRNA aqueous phase mixing ratio and manufacturing speed are both widely reported as critical process parameters for LNP production (e.g. [6–9]).

When devising a production pathway for LNPs and nanomedicines, selecting a manufacturing platform becomes a pivotal consideration. The choice between single-use and reusable systems is a crucial factor influencing efficiency, cost, and sustainability. Single-use systems offer advantages in terms of reduced cross-contamination risk, reduced downtime for cleaning, and increased flexibility in adapting to varying production scales. They eliminate the need for time-consuming and resource-intensive cleaning processes between batches. However, the extensive use of plastics drives up costs, can present supply-chain issues in times of high demand and can require the extraction of leachables to be validated, including the ethanolic stream. On the other hand, reusable systems can offer long-term cost savings, environmental sustainability, and can support the fundamental principles of green biomaterials [10].

Received: February 15, 2024. Editorial Acceptance: September 11, 2024

In our research, we explored the application of a stainless-steel crossflow membrane micromixing unit for mRNA–LNP production. We initially employed the Micropore Pathfinder™20 to determine desired manufacturing process conditions, followed by using the AXF™mini to test a range of LNP compositions before transitioning to the AXF™one for high-speed mRNA–LNP production. All three platforms share a standard design irrespective of scale: a flow-cell body housing a cylindrical membrane with a square array of pores created through laser drilling to enhance mixing. Membrane-based production systems, such as these platforms, offer scalability and precise processes by controlling flux, flow rates, and pore sizes [11, 12]. These systems have been used to produce liposomes, polymer nanoparticles, nanocrystals, and more [13–16]. A particular advantage is that these membranes are made of stainless steel and, therefore, are reusable due to their robustness, chemical compatibility, and ability to undergo repeated sterilization processes.

In the formation of nanoparticles, the ethanolic phase containing the lipids is injected through the membrane pores from the outside of the membrane. The continuous phase 'anti-solvent', usually an aqueous solution, flows through an annulus in the centre of the membrane (Fig. 1). It generates a wall shear that provides energy for the mixing process (Equation 1) where $r2$ is the radius of the outer annulus wall (i.e. the membrane), $r1$ is the radius of the inner annular wall, and (–dP/dz) is the axial pressure gradient [17].

$$\tau = \frac{r_2}{2}\left(-\frac{dP}{dz}\right)\left[1-\left(\frac{1-(r_2/r_2)^2}{2\ln(r_2/r_1)}\right)\right]$$

Equation 1

The shear in a crossflowing system has been shown to affect the resultant particle size in nanoprecipitation/self-assembly processes [18]. In this case, shear can be controlled by adjusting the volumetric flow rate (Q; Equation 2) and annular size, allowing for multiple modalities of process control, where μ is the coefficient of liquid viscosity [17].

$$Q = \frac{\pi(r_2^2 - r_1^2)}{8\mu}\left(-\frac{dP}{dz}\right)\left[r_2^2 + r_1^2 - \frac{r_2^2 - r_1^2}{\ln(r_2/r_1)}\right]$$

Equation 2

Therefore, our studies aimed to test this manufacturing technology to produce mRNA–LNPs at a small (1 ml) scale through to GMP production rates (500 ml/min). To achieve this, we first optimized our production of LNPs at a small scale using a standard LNP composition before testing the efficacy of three different LNPs in small-scale mouse studies. Finally, we produced an mRNA–LNP vaccine batch at GMP production speeds. Across all platforms, performance was commensurate with conventional microfluidic and jet mixers.

Materials and methods

Materials

Dimethyldioctadecylammonium (Bromide Salt) (DDAB) and 1,2-dimyristoylrac-glycero-3-methoxypolyethylene glycol-2000 (DMG-PEG2000) were sourced from Avanti Polar Lipids (Alabaster, AL, USA). 1,2-distearoyl-sn-glycero-3-phosphocholine (DSPC) was obtained from Lipoid

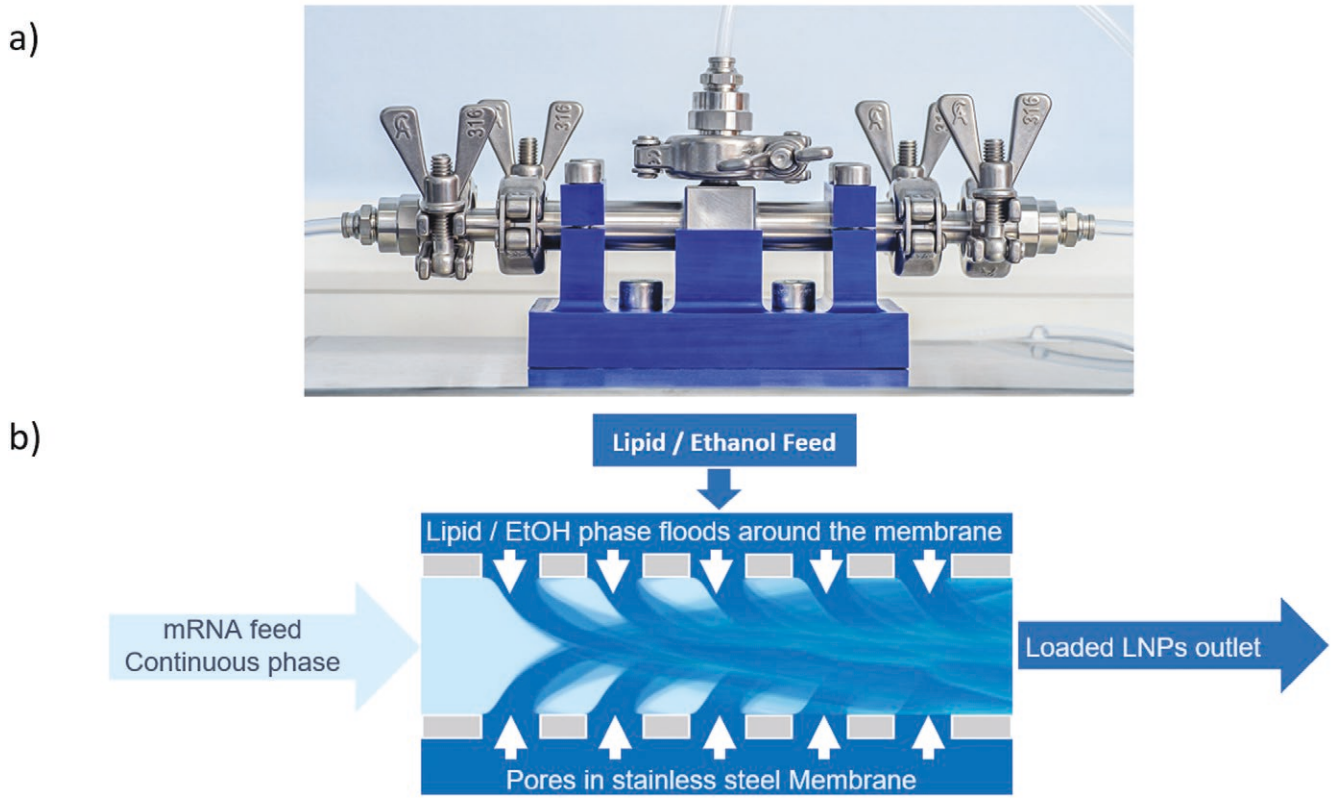

Figure 1. Schematic illustrating the action of the crossflow membrane micromixing unit in forming nanoparticles: (a) external image of the unit and (b) the crossflow membrane mixing process.

(Ludwigshafen, Germany). Cholesterol (Chol), citric acid, sodium citrate tribasic dehydrate, and polyadenylic acid (PolyA) were acquired from Merck Life Science (Hertfordshire, UK). Phosphate-buffered saline tablets (PBS pH 7.4) were obtained from Oxoid Ltd. (Basingstoke, UK). Tris (hydroxymethyl) aminomethane (TRIS-base), DilC18(7), and ethanol (EtOH) were procured from Fisher Scientific (Loughborough, UK). The One-Glo luciferase Assay system and D-Luciferin+K (VivoGlo Luciferin) were purchased from Promega Ltd. (Chilworth, UK). The ionizable lipids Heptadecan-9-yl 8-{(2-hydroxyethyl)[6-oxo-6-(undecyloxy)hexyl]amino} octanoate (SM-102), 4-hydroxybutyl)azanediyl]di(hexane-6,1-diyl) bis(2-hexyldecanoate (ALC-0315) and 1,1′-[[2-[4-[2-[[2-[*bis*(2-hydroxydodecyl)amino]ethyl](2-hydroxydodecyl) amino]ethyl]-1-piperazinyl]ethyl]imino]*bis*-2-dodecanol (C12-200) was acquired from Broadpharm (San Diego, CA, USA). Messenger RNA encoding Luciferase (EZ Cap Firefly Luciferase mRNA (5-moUTP), R1013-APE) was obtained from Stratech Scientific (St. Thomas' Place, Cambridgeshire, UK). Ovalbumin-encoding mRNA [1] modified with 5-methoxyuridine (5 moU) (MRNA41) was purchased from OZ Bioscience (Marseille, France). Goat anti-Mouse IgG (H + L) Secondary Antibody HRP (A16066) was bought from Invitrogen (MA, USA). Goat Anti-Mouse IgG2a-HRP (1081-05) and Goat Anti-Mouse IgG1-HRP (1071-05) were gained from Southern Biotech. Quant-it Ribogreen RNA assay kit and 1,1-dioctadecyl-3,3,3,3-tetramethylindotricarbocyanine iodide (DiR) were purchased from Invitrogen (MA, USA). Minimal Essential Medium, foetal bovine serum, sodium pyruvate, and penicillin/streptomycin were acquired from Gibco, Thermo Fisher Scientific (NY, USA). All solvents and chemicals were of analytical grade, and the in-house system provided milliQ-water.

Formulation of lipid nanoparticles (LNPs)

LNPs were prepared using the Micropore Pathfinder™20, AXF™mini or AXF™one from Micropore Technologies Ltd. (Redcar, UK), which uses a precision-engineered tubular membrane. Lipid stocks were prepared individually in ethanol. Cationic lipid nanoparticles were composed of DSPC:Chol:DOTAP/DDAB:DMG-PEG2000, whereas ionizable lipid nanoparticles were composed of DSPC:Chol:Ionizable lipid:DMG-PEG2000 at molar ratios as outlined in Table 1. Tris buffer pH 6 10 mM or sodium acetate pH 4 50 mM was used as the aqueous phase for cationic lipid nanoparticles and ionizable Lipid nanoparticles, respectively.

The lipid phase, at a concentration of 3–4 mM in ethanol, was paired with the aqueous phase containing polyA or mRNA in the appropriate buffer, maintaining a N/P ratio of 6 (molar ratio of amine groups of the ionizable lipid to phosphate groups on mRNA). For the Pathfinder studies, the influence of the aqueous to organic ratio (FRR; 1:1 to 5:1) and the production speed (TFR; 10–100 ml/min) was assessed for a range of LNPs encapsulated with PolyA in the appropriate buffer. mRNA encoding ovalbumin [1] and Firefly luciferase (Fluc) were used for the immunization and expression studies, respectively. Additionally, 1% mol of DiR, a lipophilic fluorescent dye, was incorporated in the organic phase to trace LNPs' *in vivo* biodistribution. A 3:1 flow rate ratio (FRR) was maintained while the production speed varied. Post self-assembly, LNPs were purified either through dialysis (MWCO 12 000–14 000 Da, Merck Life Science, Hertfordshire, UK) against 200 ml PBS or spin column (Amicon® Ultra-15 Centrifugal Filter Unit, 100 kDa). The purification involved diluting samples 40 times in PBS pH 7.4 and centrifuging at 2000 g at 4°C until the required volume was obtained.

LNP characterization: particle size, polydispersity, and zeta potential

Particle size (*z*-average hydrodynamic diameter), polydispersity index (PDI), and zeta potential were measured by dynamic light scattering using a Zetasizer Ultra (Malvern Panalytical Ltd, Worcestershire, UK) equipped with a 633 nm laser and detection angle of 173°. Samples were diluted to 0.1 mg/ml lipid concentration with PBS to measure particle size and PDI and with ultrapure water for zeta potential. The dispersant (PBS) refractive index (RI) and viscosity values were 1.330 and 0.8882 cP, respectively, whereas the material absorbance and RI were 0.01 and 1.49. Zetasizer Software v.7.11 (Malvern Panalytical Ltd., Worcestershire, UK) was used for data acquisition. All measurements were undertaken in triplicate with the attenuation value between 7 and 8. Mean particle size, PDI, and zeta potential are expressed as the mean ± SD.

Quantification of nucleic acid loading: poly(A) and mRNA

Nucleic acid (PolyA and mRNA) encapsulation efficiency (EE%) was measured using Quant-iT™ RiboGreen™ RNA Assay Kit (Invitrogen™, Thermo Fisher Scientific,

Table 1. Lipid composition of LNPs formulations (% molar ratio).

LNP	DSPC	Cholesterol	Cationic/ionizable lipid	PEG lipid
SM102	10	38.5	50	1.5 (DMG-PEG2000)
ALC-0315	9.4	42.7	46.3	1.6 (ALC-0159)
C12-200	16	46.5	35	2.5 (DMPE-PEG2000)
DOTAP	10	38.5	50	1.5 (DMG-PEG2000)
DDAB	10	48	40	2 (DMG-PEG2000)

Loughborough, UK). Briefly, 100 µl of the diluted fluorescent dye was added to 100 µl of diluted LNPs in the presence or absence of 1% (w/v) Triton-X and incubated in the absence of light for 15 min at 37°C. Nucleic acids were quantified by measuring fluorescence (λem = 520 nm, λex = 480 nm) using a fluorimeter (Polarstar Omega, BMG Labtech). A linear calibration curve up to 1500 ng/ml was obtained ($R^2 \geq 0.998$) for each of the nucleic acids tested. The encapsulation efficiency (%) was calculated using the standard curve with and without Triton to quantify nonencapsulated and total mRNA concentration.

In vitro assays for cell viability, LNP uptake, and mRNA expression

Cell viability and LNP uptake assays for PolyA-loaded LNPs with 1% mole DilC18 were conducted using the HEK293 cell line. LNPs for these assays were prepared using the Micropore AXF™mini or AXF™one. In brief, 100 µl of HEK293 cells (ATTC, Passage number between 10 and 22; 80% confluence) were seeded into a 96-well plate at a density of 10^4 cells per well and incubated for 48 h at 37°C with 5% CO_2. Subsequently, cells were treated with 100 µl of LNPs at concentrations ranging from 0.25 to 2 µg/ml for 24 h, followed by incubation with 1X AlamarBlue reagent (AlamarBlue™ cell viability reagent, ThermoFisher) for 4 h or treatment with 2% Triton X in PBS for 10 min. For cell uptake, treated wells were washed with PBS to remove any access LNPs and fresh media. Cell viability was quantified by measuring the fluorescence of the plate at 570 nm and 595 nm. LNP cell uptake was quantified by measuring fluorescence intensity using the GloMax system (Promega). mRNA (FLuc) expression was conducted using HEK293 cells (80% confluence) seeded into a 96-well plate at a density of 10^4 cells per well and incubated for 48 h at 37°C with 5% CO_2. Cells were treated with LNPs at concentrations of 0.25–2 µg/ml for 24 h, followed by the addition of 100 µl of the One-Glo Luciferase assay system (Promega). Bioluminescence was quantified by measuring the total luminescence across the entire wavelength range.

Gel electrophoresis for the mRNA integrity

To assess the encapsulated mRNA in the LNPs, a total of 10 µg either naked (positive control) or mRNA encapsulated in LNPs were precipitated with 750 µl of ethanol and 25 µl of 3 M sodium acetate pH 5.2, and the samples were centrifuged at 14 000 rpm for 20 min. Ethanol precipitation and centrifugation were repeated twice. mRNA pellets were resuspended in 35 µl of DEPC-treated water, mixed with formaldehyde load dye (1:3 v/v), heated at 65°C for 10 min and then cooled to room temperature. Then, the equivalent of 400 ng of mRNA (7 µl) was loaded in a denatured 1% agarose gel in Northern Max 3-(N-morpholino)propane sulfonic acid (MOPS) running buffer containing 0.1% of SYBR gold stain and run at 90 V. Ambion Millennium marker was used as the molecular weight standard. Gel images were acquired in a Gel Doc EZ imager (Bio-Rad).

In vivo mRNA–LNP expression and biodistribution studies

In the first In Vivo Imaging System (IVIS) study, Fluc mRNA–LNPs were prepared with three different ionizable lipids using the Micropore AXF™mini (SM-102, ALC-0315, or C12-200), for the initial screening of LNPs to assess the expression profile of Fluc mRNA. Two independent studies were conducted with groups of three female BALB/c mice and one control BALB/c mouse (10–12 weeks old). Mice were injected with 5 µg/50 µL of mRNA–LNPs per leg via the intramuscular (i.m.) route. Mice then received a subcutaneous (s.c.) injection of D-luciferin (150 mg/kg) post injection and 6 h after the i.m. injection of LNPs. Ten minutes after receiving D-luciferin, they were anaesthetized with 3% isoflurane and transferred to the IVIS cabin, maintaining the isoflurane level at 1%. They were imaged in an open filter using an *in vivo* imaging system (IVIS Spectrum, Perkin Elmer). The total flux (p/s) was gained using the region of interest tool for each mouse using Living Image software. The average of total flux was calculated.

In the second study, LNPs were made using the Micropore AXF™one. Fluc mRNA loaded SM-102 LNPs and incorporating 1% lipophilic fluorescent dye 1,1′-dioctadecyl-3,3,3′,3′-tetramethylindotricarbocyanine Iodide (DiR) were used to investigate the *in vivo* retention of LNPs at the injection site and mRNA expression. Groups of five (6–9-week-old) female BALB/c mice were injected with 5 µg/50 µl intramuscularly in both quadricep muscles. Mice imaging was carried out using an IVIS Spectrum (Perkin Elmer) and Living Image software for data capture and analysis. The presence of DiR was detected using an excitation wavelength of 710 nm and an emission filter of 780 nm. Mice then received a subcutaneous (s.c.) injection of D-luciferin (150 mg/kg) before the time points for bioluminescence imaging, and the mRNA expression was detected using the bioluminescence at the emission wavelength firefly luciferase (560 nm). A medium binning and f/stop of 2 was used, and acquisition time was determined for each image with auto-exposure settings. Mice were anaesthetized for imaging using 3% isoflurane. Anaesthesia was maintained during imaging at 1% isoflurane. Images were taken after administration of formulations at time 0, 6 h, 1, 2, 3, 6, and 9 days post injection. The total flux (p/s) was calculated for each mouse. All mice were housed under conventional conditions (22°C, 55% humidity, 12 h day/night cycle) in their experimental cage and were given a standard diet *ad libitum*.

Immunization studies

Groups of five (6–9 weeks old) female BALB/c mice were immunized intramuscularly on days 0 and 28 in their right quadricep (50 µl) with (5 µg/dose) mRNA encoding for ovalbumin [1] formulated in SM-102 LNPs were prepared using the Micropore AXF™one or free mRNA encoding for ovalbumin. Mice were dosed (5 µg/50 µl) via intramuscular injection with a prime (day 0) and booster (day 28). The serum was collected via tail bleeding 27 days after the first injection and two weeks after the second injection (day 42), and the antibody endpoint titres were detected via ELISA. Cytokine (IL-5 and IFN-g) splenocyte production was also measured. Sera was collected by spinning the collected blood samples by centrifugation at 10 000 rpm for 10 min. Sera stored at –20°C. Spleens from all mice were collected 2 weeks after the second immunization to perform a T-cell assay *in vitro*.

Specific IgG isotype responses

Blood samples were collected over the course of the study and assessed for serum-specific IgG isotype (Total IgG, IgG1, and IgG2a) antibody titre levels. Briefly, 96-well micro-titre plates

(Greiner Bio-One GmbH, Frickenhausen, Germany) were coated with 100 µl (1 µg/ml PBS pH 9.0) of albumin from chicken egg white [1] (Merck Life Science, Hertfordshire, UK) overnight at 4°C. The plates were then washed three times with wash buffer (PBS pH 7.4/0.05% v/v Tween-20). Subsequently, the plates were blocked by adding 150 µl of Marvel® solution (4% w/v in PBS pH 7.4) to the appropriate wells of the plate, and the plates were incubated for 1 h at 37°C. The plates were washed three times in wash buffer, and then 100 µl of the relevant serum sample, serially diluted in PBS buffer from 1:100 or higher depending on the experiment, was added to the appropriate wells of the plate. The plates were incubated as before for 1 h, washed three times in wash buffer, and 100 µl/well of horseradish peroxidase (HRP) conjugated goat anti-mouse Total IgG, IgG1 or IgG2a used of 1:2500, 1:20 000 or 1:5000, respectively dilution (PBS pH 7.4/10 % v/v FCS) was added to the appropriate wells of the plate. The plates were incubated for 1 h as before, washed three times with wash buffer, and 100 µl/well of 3,3′,5,5′-tetramethylbenzidine (TMB) substrate (Fisher Scientific, Loughborough, UK) added. The reaction was stopped after 20 min by adding 50 µl/well of 10% aqueous sulfuric acid. The absorbance of the wells was measured at 450 nm using a Microplate Manager® Device (Bio-Rad Laboratories, Inc, CA, USA), and the mean endpoint ± standard error of the mean [10] for each group was determined.

Lymphocyte proliferation studies

Spleens were removed from mice at sacrifice under aseptic conditions, and single-cell suspensions were prepared in incomplete RPMI-1640 medium (RPMI-1640, 100 µg/ml penicillin/streptomycin and 200 mM L-glutamine). The spleen was passed through a Nitex filter using the end of a 2.5 ml syringe, and the resulting cell suspension was transferred to a labelled universal tube. The cells were pelleted by centrifuging at 300 × *g* (BioFuge Fresco, Heraeus instruments, supplied by Thermo Scientific, Hemel Hempstead, UK) for 5 min at 4°C. The spleen cell pellet was resuspended in 3 ml Boyle's solution (0.007 M NH_4Cl, 0.0085 M Tris, pH 7.2) and the resulting suspension was incubated for 5 min at room temperature. The spleen cell suspension was centrifuged as before for 5 min, and the cells were resuspended in a 5 ml RPMI-1640 medium. This process was repeated to ensure that all of Boyle's solutions had been removed. Cells were then resuspended in 1 ml RPMI-1640 complete medium (incomplete RPMI-1640 medium supplemented with 10% v/v foetal calf serum), and the cell concentration was determined. In all cases, cell viability was > 97%. Spleen cells (5×10^5/well) were added to the appropriate wells of a 96-well tissue culture plate and incubated with medium alone (unstimulated controls) or soluble antigen (5 µg/ml PBS pH 7.4 OVA) or concanavalin A (10 µg/ml, positive control) in a final volume of 200 µl. Plates were incubated for 72 h at 37°C in an atmosphere of 5% carbon dioxide and 95% air. After 72 h, the plates were stored at –20°C until cytokine levels could be determined.

Cytokine determination

Cytokine levels in the cell supernatants were measured using an ELISA assay using anti-mouse cytokine antibodies and cytokine standards. Briefly, a 96-well ELISA plate was coated with 50 µl/well of the appropriate rat anti-mouse anti-cytokine antibody (IL-5 or IFN-γ, 2 µg/ml, in coating buffer [PBS pH 9]). Plates were incubated overnight at 4°C and then washed three times in wash buffer (PBS pH 7.4 containing 0.05% v/v tween-20). Plates were then blocked by adding 150 µl PBS pH 7.4 containing 10% v/v FCS to the appropriate wells of the plate, and plates were incubated for 1 h at 37°C. Plates were washed as before, and then 30 µl of cell supernatant or cytokine standard (serially diluted from 20 ng/ml with 10% v/v FCS in PBS pH 7.4) were added to the appropriate wells of the plate before incubating as before for 2 h. Plates were washed as before, and then 100 µl of the appropriate rat anti-mouse biotin anti-cytokine antibody (1 µg/ml, 10% v/v FCS in PBS pH 7.4) were added to the appropriate wells of the plate. Plates were incubated for 1 h as before and then washed three times. Streptavidin horseradish peroxidase (HRP) conjugated (100 µl, 1:4000 in 10% v/v FCS in PBS pH 7.4) was added to the appropriate wells of the plate before incubation for an hour at 37°C. Plates were washed as above, and then 100 µl of TMB substrate was added to the appropriate wells of the plate before incubating at room temperature in the dark for 20–60 min. The absorbance of the samples at 405 nm was measured, and the amount of cytokine present (ng/ml) in the cell supernatants was determined from the standard curve plotted from standards run on the same plate. The mean cytokine production (ng/ml ± SEM) for each treatment was determined.

Ethics statement

Animal experiments and experimental procedures were carried out in line with UK Home Office regulations and the University of Strathclyde Animal Welfare and Ethical Review Board regulations under project license number PPL PP1650440. BALB/c mice were all bred and maintained in the Biological Procedures Unit at the University of Strathclyde, Glasgow and experimental design and reporting adhere to the ARRIVE guidelines.

Statistical analysis

Results are represented as mean ± SD (phyisco-chemical characteristics) and SEM (*in vivo* studies) of at least $n = 3$ independent batches. ANOVA tests were used to assess statistical significance, combined with the Kruskal–Wallis test followed by Dunn's *ad hoc* to determine differences between treatments using GraphPad software; a (P-value < .05) was considered significant.

Results

Optimization of production parameters for mRNA–LNPs using crossflow technology

Initially, we investigated the effect of flow rate ratio and total flow rate production parameters on polyA-loaded LNPs phyisco-chemical properties using three different LNP formulations—a cationic lipid-based LNP prepared using DOTAP and two ionizable LNP formulations based on SM102 and C12-200 (Table 1). The results in Fig. 2 show that at low mixing ratios (1:1), the LNP particle sizes are large and heterogeneous across the three LNP formulations evaluated, irrespective of the speed. Increasing the mixing ratio to 3:1 or above, reduced particle sizes and PDI values to generally <100 nm and <0.2 PDI, respectively (Fig. 2a–c). This aligns with prior investigations where the tuning of the

ethanol concentration has been considered to control particle size (e.g. [8, 9].). While the production speed can be seen to have less of an impact, at 10 ml/min, the particle size tended to be higher than at the high speeds assessed (55 ml/min and 100 ml/min). Neither the mixing ratio nor the production speed made a notable difference regarding zeta potential. However, the LNPs made with DOTAP (a fixed cationic lipid) tended to have a slight positive zeta potential compared with the ionizable lipids (SM102 and C12-200), which had a slight anionic charge (Fig. 2d—f). Finally, in terms of encapsulation efficiency (Fig. 2g–i), efficiency was lower for the 1:1 mixing ratio irrespective of the production speed and LNP composition, while at 3:1 and 5:1 %, EE was consistently >95% across all three LNPs. Based on these results, a mixing ratio of 3:1 was adopted for all subsequent studies.

Testing optimized parameters across a range of LNP formulations

The next step was to manufacture a range of LNPs at bench-scale to support *in vitro* analysis and a pilot *in vivo* study. LNPs (2 ml batch size) were prepared using the AXF™mini at a flow rate ratio of 3:1 (citrate buffer:ethanol) at a 30 ml/min production speed. Our initial experiments (Fig. 2) assessed production speeds at three distinct flow rates: 10, 55, and

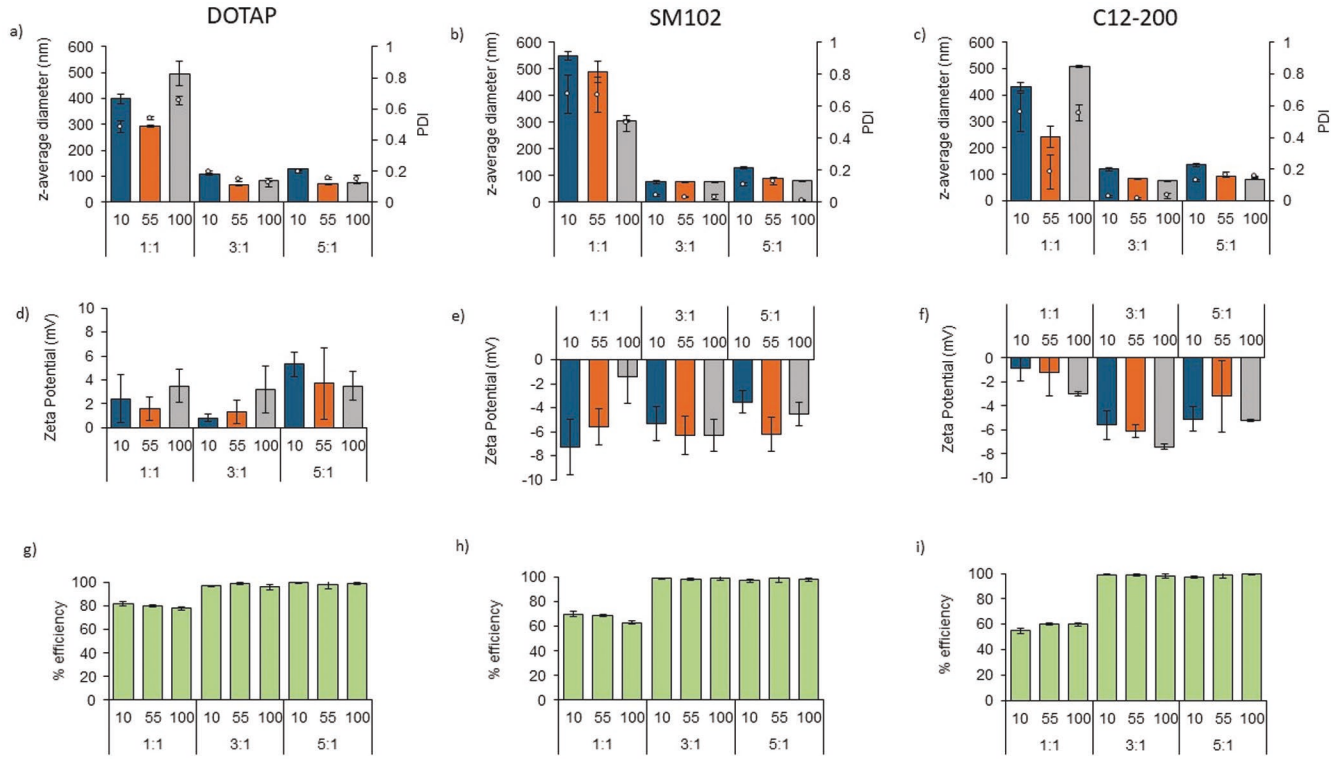

Figure 2. The effect of the flow rate ratio and total flow rate on LNPs *z*-average size, PDI, zeta potential, and encapsulation efficiency (%). PolyA was used as the payload in these studies. LNPs were produced using Micropore Pathfinder™. DOTAP, SM102, or C12-200 LNPs (see Table 1 for full compositions) were prepared at a flow rate ratio of 1:1, 3:1, or 5:1 and a production speed of 10, 55 or 100 ml/min to a final polyA concentration of 0.0213 mg/ml before ethanol removal. LNPs were purified to remove ethanol via dialysis. Results represent the mean ± SD of 3 independent studies.

Table 2. Production of LNPs using AXF™mini. LNPs were prepared using the AXF™mini at a flow rate ratio of 3:1 (citrate buffer 50 mM pH4:ethanol) at a 30 ml/min production speed to a final mRNA concentration of 0.0213 mg/ml before ethanol removal. LNPs were purified to remove ethanol and concentrated to the required mRNA concentration via spin-column purification. Results represent mean ± SD of 3 independent studies.

LNP	Payload	*z*-Average diameter	PDI	Zeta potential (mV)	%EE
SM102	polyA	80 ± 4	0.13 ± 0.01	–0.9 ± 10	99 ± 1
ALC-0315	polyA	95 ± 3	0.13 ± 0.02	–7.5 ± 2	93 ± 2
C12-200	polyA	73 ± 1	0.16 ± 0.01	–7.6 ± 1	99 ± 1
DOTAP	polyA	74 ± 3	0.15 ± 0.01	–1.7 ± 1	100 ± 1
DDAB	PolyA	92 ± 1	0.13 ± 0.03	–3.7 ± 5	85 ± 2
SM102	FLuc mRNA	94 ± 7	0.11 ± 0.06	–5.6 ± 1	98 ± 1
ALC-0315	FLuc mRNA	93 ± 1	0.18 ± 0.02	–8.7 ± 1	95 ± 2
C12-200	FLuc mRNA	99 ± 1	0.13 ± 0.04	–6.7 ± 2	99 ± 2
SM102	OVA	105 ± 1	0.05 ± 0.04	–6.1 ± 4	99 ± 2

100 ml/min. The data indicated that particle sizes within our desired CQAs were achieved between 10 and 55 ml/min flow rates. Therefore, we selected an intermediate flow rate of 30 ml/min to balance scalability and practicality at lower bench-scale volumes. The results in Table 2 confirm that a wide range of LNP compositions can be manufactured both using polyA (a useful low-cost mRNA surrogate) or mRNA (encoding FLuc or OVA; average MW, 672 kDa and 451 kDa, respectively) (Table 2).

The SM102-based LNPs were also further tested for mRNA integrity, *in vitro* cell viability and mRNA expression in HEK293 cells (Fig. 3). To measure mRNA integrity, mRNA was extracted from LNPs and analysed through gel electrophoresis (Fig. 3a). *In vitro*, HEK293 cells were incubated for 24 h with SM-102 lipid nanoparticles containing firefly luciferase mRNA at varying concentrations (0.5–2 μg/ml mRNA dose). Subsequently, we assessed cell viability and relative luminescence intensity through an *in vitro* luciferase assay (Fig. 3b and c). The results in Fig. 3a show that the mRNA remains intact, and the LNPs are not toxic in the concentration range tested in the HEK293s (Fig. 3b) and promote mRNA protein (luciferase) expression (Fig. 3c).

Given these results, three LNP formulations based on SM102, ALC-0315, and C12-200 using the Micropore AXF™mini (Table 1) were also tested in a small-scale mouse study to measure mRNA protein (luciferase) expression using mRNA encoding luciferase (Fluc). The bioluminescence profile of Fluc-mRNA LNPs was analysed using the IVIS system at 10 min and 6 h after injection of the LNPs (Fig. 4). BALB/c mice were injected with 5 μg (mRNA) of Fluc mRNA–LNPs into each leg via the i.m. route. The results in Fig. 4 show all three formulations giving *in vivo* expression, with SM102 and ALC-0315 LNPs giving strong expression compared with mRNA formulated in C12-200 LNPs (Fig. 4). This is in line with [19], where FLuc expression of mRNA in SM102 and ALC-0315 LNPs was also studied. These results confirm the efficacy of the LNPs both *in vitro* and *in vivo*.

Scaling up LNP manufacture to GMP production speeds

Given the proven efficacy of the LNPs produced by crossflow mixing, the next step was to scale this production up to GMP scales. To do this, we initially tested a range of production speeds from 200 to 500 ml/min produced in the Micropore AXF™one. In this study, we used DDAB-based LNPs (Table 1) incorporating PolyA as an mRNA surrogate. Due to pump limitations, the maximum speed we could text was 500 ml/min; however, the system can run up to 2000 ml/min with

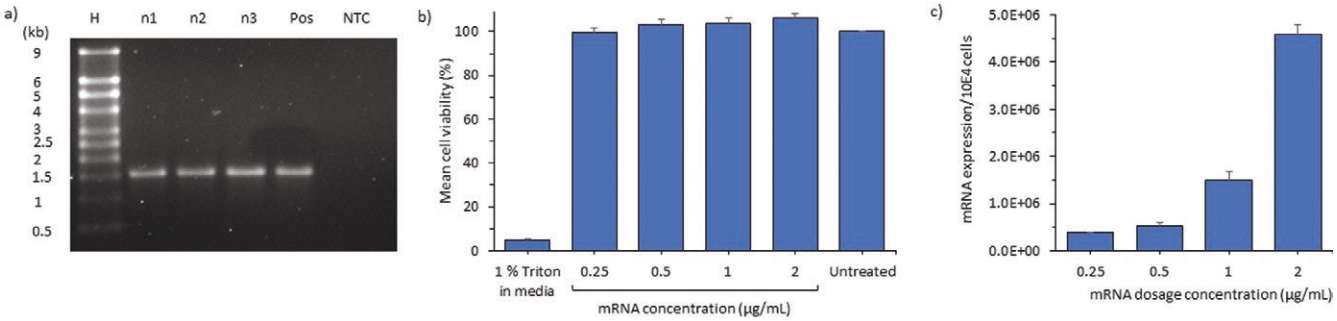

Figure 3. LNPs produced using AXF™mini *in vitro* efficacy. SM102 LNPs were prepared using the AXF™mini at a flow rate ratio of 3:1 (citrate buffer 50 mM pH4:ethanol) at a production speed of 30 ml/min to a final mRNA concentration of 0.0213 mg/ml before ethanol removal. LNPs were purified to remove ethanol and concentrated to the required mRNA/polyA concentration via spin-column purification. These LNPs were then tested in terms of (a) mRNA integrity (RNA Millenium Marker hyperladder, *n*1–3 are replicate samples, Pos: Fluc mRNA positive control, NTC: no template control), (b) HEK293 cell viability (polyA as the payload), and (c) protein (luciferase) expression. Results represent mean ± SEM of 3 independent studies.

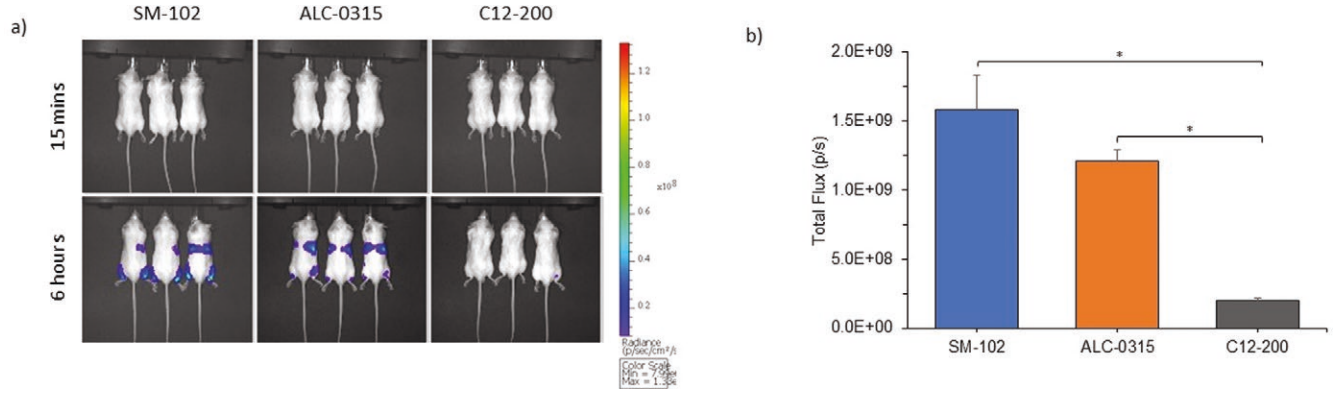

Figure 4. *In vivo* expression profile of LNPs encapsulated Fluc mRNA prepared with SM-102, ALC-0315 and C12-200 as ionizable lipids. (a) Representative IVIS images of 3 female BALB/c mice injected with 5 μg Fluc mRNA–LNP intramuscularly. (b) Quantification of the bioluminescent signal at the injection site and liver 6 h after the LNPs injection. LNPs were produced using AXF™mini at a flow rate ratio of 3:1 at a 30 ml/min production speed. Data is expressed by mean ± SEM (6 mice per formulation split over 2 independent studies) followed by conducting ANOVA combined with nonparametric tests using GraphPad Prism (*$P < .05$).

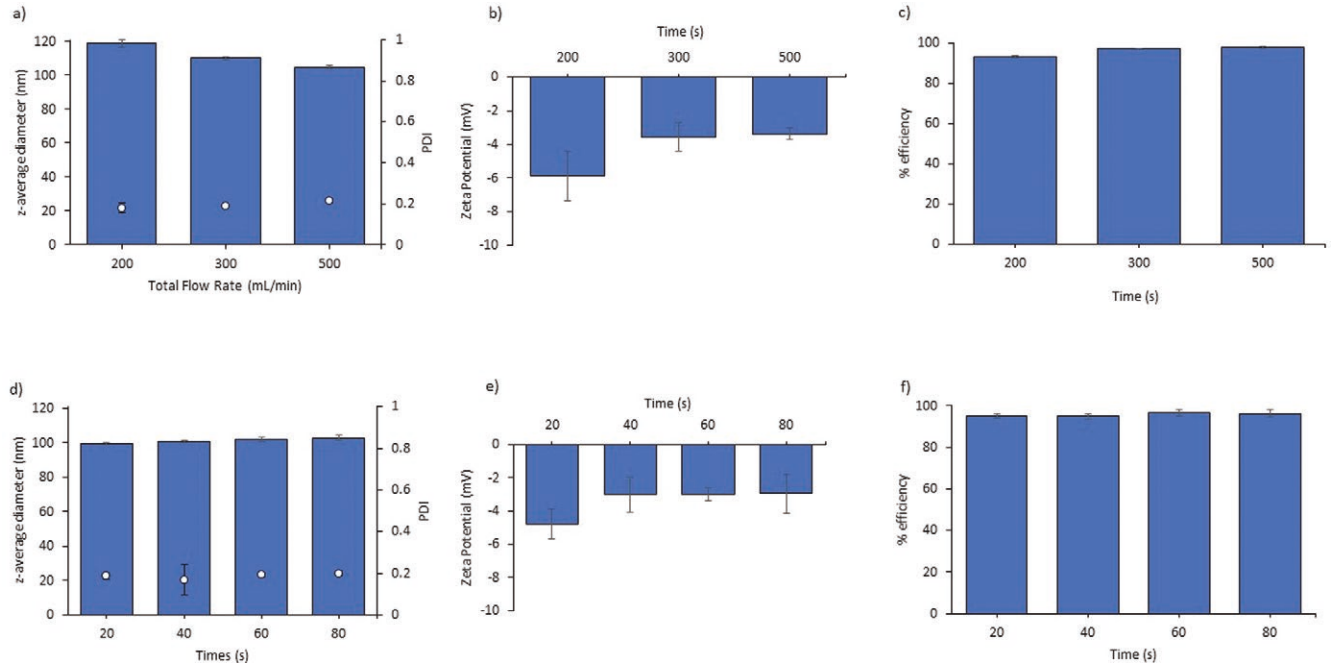

Figure 5. Physiochemical properties of LNPs produced using AXF™one. DDAB LNPs were prepared using the AXF™one at a flow rate ratio of 3:1 (citrate buffer 50 mM pH6:ethanol) to a final polyA concentration of 0.0213 mg/ml before ethanol removal. PolyA was used as a surrogate for mRNA in this study. These LNPs were then studied for the effect of total flow rate (200, 300, or 500 ml/min); (a) LNPs *z*-average size, PDI, (b) zeta potential, and (c) encapsulation efficiency (%). Consistency of the product produced at a flow rate of 500 ml/min on LNP production was then tested by collecting samples at different time points (20, 40, 60, and 80 s); (d) LNP *z*-average size, PDI, (e) zeta potential, and (f) encapsulation efficiency (%). Results represent the mean ± SD of 3 independent studies.

appropriately rated pumps. The results in Fig. 5 demonstrate that increasing the production speed from 200 ml/min to 500 ml/min reduced the particle size of these DDAB-LNPs from ~120 nm to 100 nm (Fig. 5a), and across these production speeds, the zeta potential was similar (~0 to—8 mV; Fig. 5b), and encapsulation efficiency was high (>95%; Fig. 5c). We also tested the reproducibility of the LNPs during production. Fig. 5d–f demonstrate product reproducibility across the time range tested. These results confirm the ability to scale from the AXF-mini through to the large-scale AXF-one without changing process parameters. Thus, based on these results, we further progressed to manufacturing an mRNA–LNP batch for testing in a preclinical (mouse) protein expression and vaccine study.

Analysis of mRNA–LNP clearance and protein expression following intramuscular administration

The phyisco-chemical attributes and *in vitro* expression were initially confirmed for SM102-based LNPs produced at 500 ml/min production speeds and the selected 3:1 flow rate ratio (Fig. 6). mRNA encoding luciferase (Fluc) was used in Fig. 6 studies. Again, the results show that the SM102 LNPs were within our required CQAs (Fig. 6a), with demonstrated cell uptake (Fig. 6b), high cell viability (Fig. 6c) and mRNA protein (luciferase) expression (Fig. 6d). Given the LNPs produced at this GMP scale (Fig. 6) mapped to our small-scale studies (Table 2), these results confirmed the efficacy of LNPs produced at high (500 ml/min) volume, and thus, we progressed to *in vivo* studies. BALB/c mice were intramuscularly injected with DiR-labelled LNPs encapsulating 5 µg of mRNA encoding luciferase (Fluc) to study this. By using DiR-labelled mRNA–LNPs, we can track both the biodistribution of LNPs (by imaging the mice under a DIR fluorescence filter) and mRNA luciferase expression (via bioluminescence imaging) [20].

Figure 7 shows the biodistribution and expression profile of LNPs encapsulated F-Luc mRNA. Figure 7a shows the IVIS images of BALB/c mice intramuscularly injected with either 5 µg DiR labelled Fluc mRNA–LNPs or mRNA (without LNPs) over 9 days. These results are then plotted as fluorescence over time (Fig. 7b) and bioluminescence over time (Fig. 7c). Fig. 7a and b show that the mRNA–LNPs are retained at the injection site over the 9 days of the study, while no fluorescence is detected with mRNA alone, as would be expected given there is no lipid content. When considering mRNA expression (Fig. 7c), no expression for mRNA administered without a delivery system is detected. In contrast, luciferase expression is detected over 48 h when delivered using SM102 LNPs with peak fluorescence intensity (Cmax) measured 6 h after mRNA–LNP injection (Fig. 7c). These results confirm that mRNA without a delivery system is ineffective and that mRNA–LNPs produced at 500 ml/min in the crossflow mixer promoted high levels of mRNA-encoded expression and mapping to our small lab-scale batches.

Immune responses in mice after mRNA–LNP immunization

To study the efficacy of mRNA–LNP vaccines produced at 500 ml/min using the Micropore AXF™one, BALB/c mice were immunized with LNPs entrapping mRNA encoding the model antigen OVA. To achieve this, mRNA SM102 LNPs (as outlined in Table 1) were compared with nonformulated mRNA (Fig. 8). When comparing the responses between mRNA and mRNA–LNPs produced at 500 ml/min, the

a)

SM102 LNPs	
Size	101 ± 2 nm
PDI	0.12 ± 0.06
Zeta Potential	- 3.5 ± 1 mV
Encapsulation Efficiency	99 %

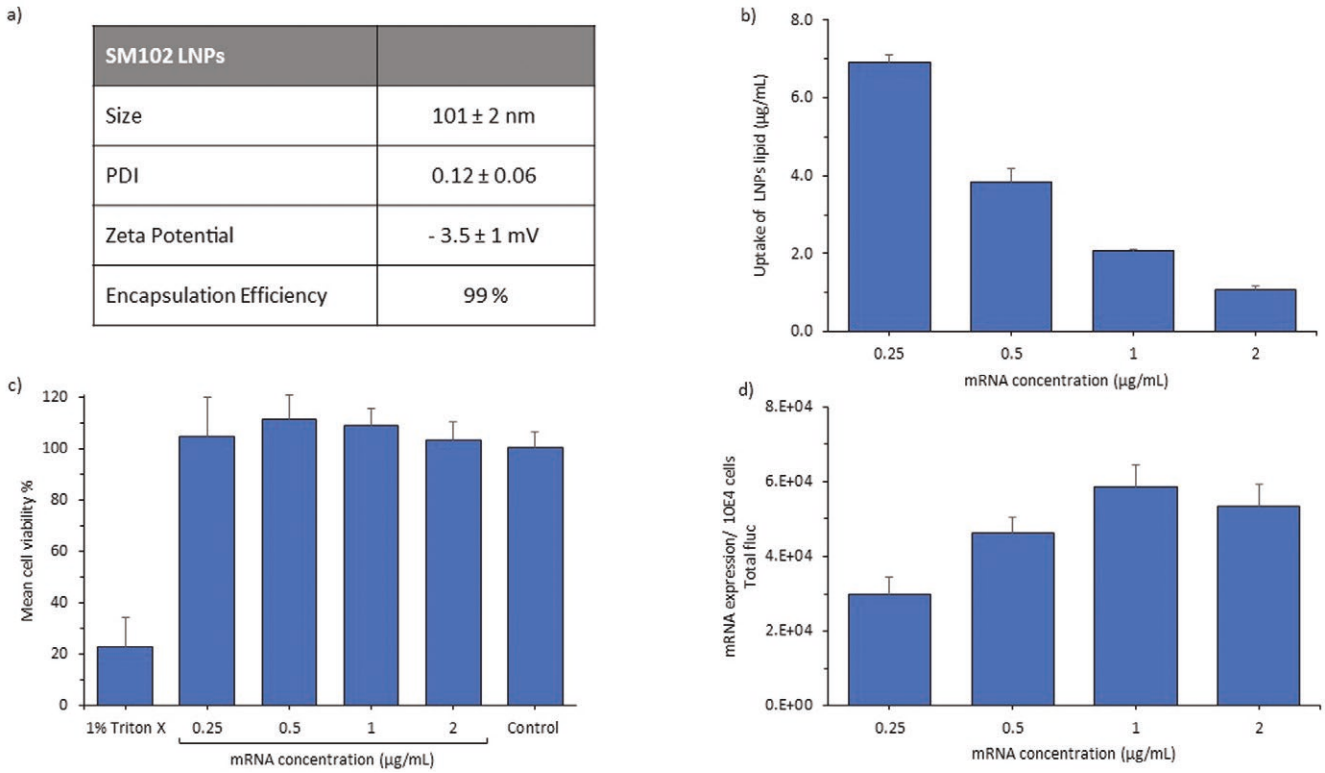

Figure 6. LNPs produced using AXF™one *in vitro* efficacy. SM102 LNPs were prepared at a flow rate ratio of 3:1 (citrate buffer 50 mM pH4:ethanol) at a production speed of 500 ml/min to a final mRNA (encoding luciferase) concentration of 0.0213 mg/ml before ethanol removal. LNPs were purified to remove ethanol and concentrated to the required concentration via spin-column purification. These LNPs were then tested in terms of (a) LNPs entrapping mRNA CQAs (*z*-average size, PDI, zeta potential, and encapsulation efficiency (%)). (b) HEK293 LNPs cell uptake % (using polyA as a surrogate), (c) cell viability (using polyA as a surrogate) and (d) protein (luciferase) expression. Results represent the mean ± SD of 3 independent studies.

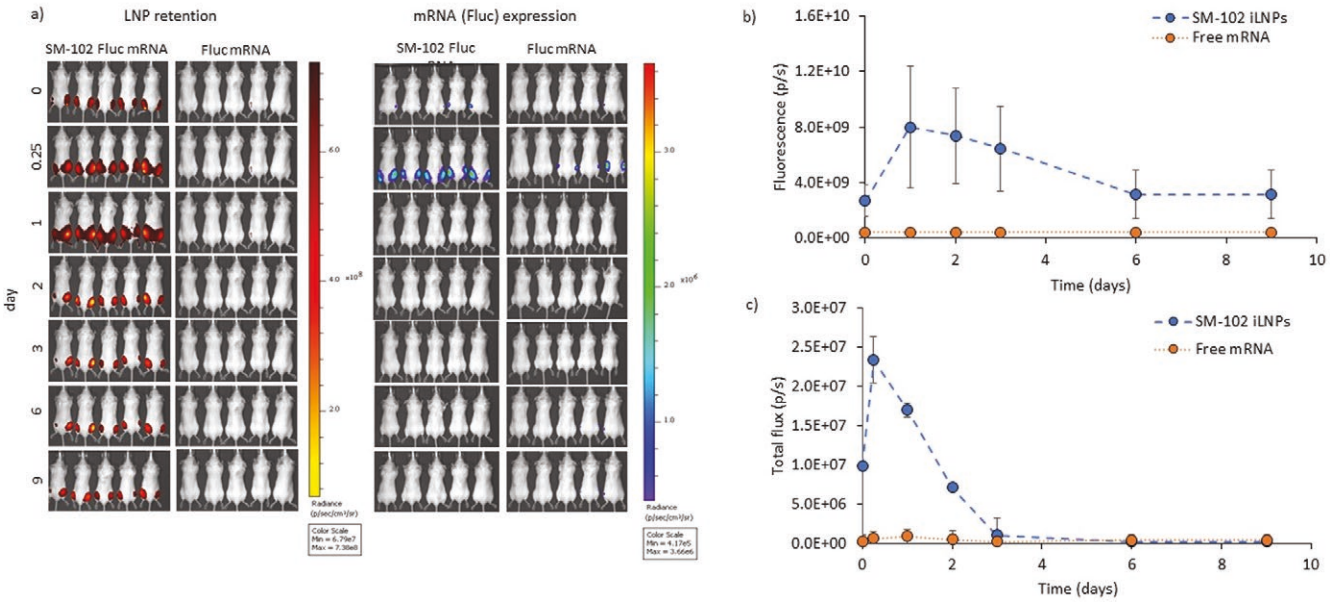

Figure 7. *In vivo* biodistribution and expression profile of LNPs encapsulated F-Luc mRNA prepared with 50 mM citrate buffer using the AXF™one. (a) IVIS images of groups of 5 female BALB/c mice injected intramuscularly with 5 µg DiR labelled Fluc mRNA–LNP and imaged at 0, 0.25, 1, 2, 3, 6, and 9 days. (b) Quantitative analysis of the fluorescence intensity in the injection site, and (c) Quantification of the bioluminescent signal at the injection site. Results represent mean ± SEM of 10 mice per formulation split over 2 independent studies (5 mice per study).

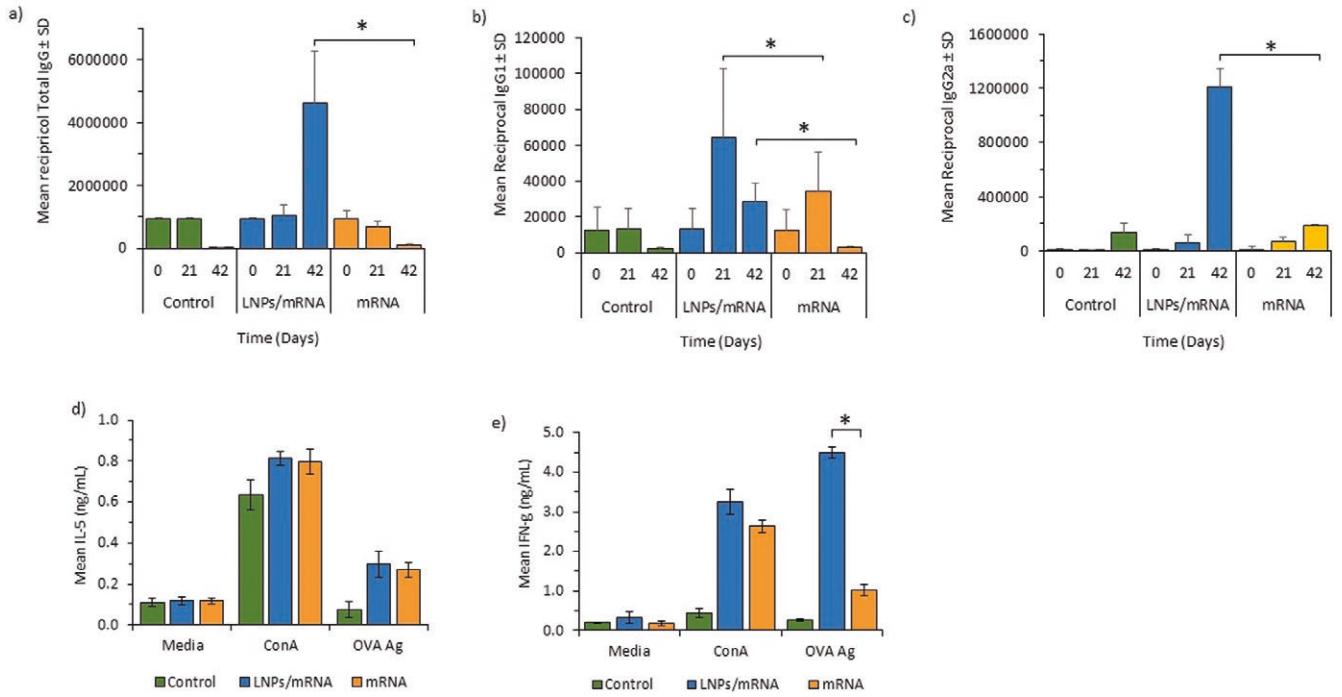

Figure 8. Vaccine potency of SM-102 LNPs encapsulated mRNA encoding OVA prepared with 50 mM of citrate buffer using the AXF™one. Groups of 5 female mice BALB/c were immunized intramuscularly on days 0 and 28 with 5 μg OVA mRNA–LNP, OVA mRNA, or nothing (control). The mice serum was then used to study the effect of vaccination on (a) the specific total IgG, (b) the specific IgG1, and (c) the specific IgG2a antibody titres. Mean (d) IL-5 and (e) IFN-g production, splenocytes (1×10^6/ml) from the same mice were incubated with medium alone (controls), ConA (10 μg/ml) or OVA soluble antigen (5 μg/ml) for 72 h. Results represent mean ± SEM of a total of 5 mice per formulation followed by conducting ANOVA combined with nonparametric tests using GraphPad Prism (*$P < .05$).

results in Fig. 8 demonstrate that at day 42, mice injected with mRNA–LNPs mounted a significantly ($P < .05$) stronger IgGT (Fig. 8a), IgG1 (Fig. 8b) and IgG2a (Fig. 8c) responses than free mRNA and IgG1 responses were also significantly higher at day 21 (Fig. 8b)($P < .05$). Regarding cytokine responses, there was no significant difference in responses between mRNA and mRNA–LNPs after antigen stimulation (Fig. 8d); however, for IFN-g, mRNA–LNPs produced significantly ($P < .05$) higher responses compared with mRNA (Fig. 8e). These responses confirm that the mRNA–LNPs formulated at GMP production speeds can produce a strong Th1 response, while mRNA alone produced no notable responses.

Discussion

In the production of LNPs, reproducibility and scalability are key. In their production, it is widely reported that both the production speed and mixing ratio of the aqueous to alcohol are critical process parameters (CPP), impacting the critical quality attributes of LNPs. This includes particle size, polydispersity and encapsulation efficiencies [21]. Previous reports demonstrate that microfluidics is an effective tool for the manufacture of nanoparticles, offering scale-independent production of a range of polymeric and lipid-based nanoparticles (e.g. [5, 8, 22, 23].). Given the recognized CPPs for nanoparticle production, when establishing a manufacturing process for LNPs initial studies should focus on the mixing ratio and total flow rate (or production speed) [24]. Therefore, in our current study, we initially evaluated the effect of both process parameters on the particle size, PDI, zeta potential and encapsulation efficiencies of LNPs. Controlling the mixing ratio in the manufacture of LNPs allows for the control of particle size, as increasing the aqueous-to-ethanol ratio increases the polarity and narrows the organic solvent stream, which helps the formation of smaller particles due to particle fusion reduction [25]. In Fig. 2, we highlight the significance of flow rate mixing ratio as a critical process parameter in crossflow micromixing; particles produced at an FRR of 1:1 were significantly ($P < .05$) larger than those generated at higher mixing ratios. On the other hand, results showed that the FRR of 3:1 generally produced smaller particles than the other FRRs tested (Fig. 2). This is irrespective of the LNP composition tested. Similarly, at flow rate ratios of 3:1 and 5:1, increasing the speed from 10 to 55 ml/min tended to reduce the particle size, but further increasing this to 100 ml/min had no significant impact (Fig. 2). As with the mixing ratio, increasing the total flow rate can increase the rate of change in polarity and result in reduced particle sizes [25]. This confirms that the mixing ratio and total flow rate are CPPs for crossflow micromixing.

Given that we had established a production process, the next step was to widen the testing of this method using a variety of ionizable lipids and payloads (Table 2). Again, we could effectively produce a range of LNPs in the size range from 73 nm to 105 nm. All particles had monodispersed size distribution with low PDI (<.2) and neutral surface charge (Table 2). In Table 2, we also confirm that a range of different nucleic acid payloads, including PolyA (2–10 nucleotides), Fluc mRNA (average MW, 672 kDa), and OVA mRNA (average MW, 451 kDa), can be effectively encapsulated within LNPs. This has similarly been demonstrated with other

manufacturing processes where saRNA or mRNA had comparable size, PDI, and EE [26, 27]. This suggests that particle size and dispersity are predominantly controlled by the manufacturing process and the lipid composition rather than the payload.

Finally, given we had demonstrated this production process with 3 LNP formulations (Fig. 4), we further studied LNPs produced by crossflow micromixing within a scale-up process. We produced LNPs at up to 500 ml/min to achieve this. Again, we demonstrated that increasing the total flow rate from 200 to 500 ml/min reduced particle size, while the PDI, zeta potential and nucleic acid loading were unaffected (Fig. 5). We then tested LNPs produced at 500 ml/min for their *in vitro* and *in vivo* efficacy (Figs. 6 and 7), demonstrating their effectiveness across our models, in line with our small-scale batches. Across the expression profiles for the mRNA–LNPs, we see some variability (Fig. 3c vs. Fig. 6d), which can be attributed to these studies being done on different occasions with different batches of mRNA. Within Fig. 6, we also see a decrease in the uptake of LNPs with increasing LNP concentration. This is to be expected, given we are probably seeing saturation of the uptake mechanism with increasing LNP concentrations. However, a further factor in the potency of LNPs is the ability of LNPs to escape from endosomes and enter into the cytoplasm. Indeed, it has been reported that less than 5% of LNPs successfully escape from the endosomes and release their RNA payload into the cytosol. This limited escape rate significantly limits the overall efficiency of LNP-mediated delivery [28]. Finally, we vaccinated mice with SM102 LNPs encapsulation mRNA encoding OVA and measured immune responses against OVA. Our results (Fig. 8) demonstrate the efficacy of these LNPs as vaccines compared with 'free' mRNA. SM102 is the ionizable lipid used within the Spikevax® formulation manufactured by Moderna Tx Inc. and has proven efficacy in a vaccine formulation against COVID-19.

Conclusion

Our results confirm the applicability of stainless-steel crossflow membrane micromixing for the entire spectrum of mRNA–LNP production, ranging from initial discovery volumes to GMP-production scale. Exemplified by these platforms, membrane-based production systems provide scalability and precise control over the manufacturing process by regulating factors such as flux, flow rates, and pore sizes. A distinctive advantage lies in the stainless-steel composition of these membranes, allowing for reusability owing to their robustness, chemical compatibility, and the capability to undergo repeated sterilization processes. Nevertheless, the choice between single-use and reusable systems ultimately depends on specific production needs, financial constraints, and environmental considerations.

Author contributions

M.H. (Conceptualization, methodology, formal analysis, investigation, data curation, writing—original draft preparation, writing-reviewing and editing, visualization); L.O'C (Conceptualization, methodology, formal analysis, investigation, data curation, writing—original draft preparation, writing-reviewing and editing, visualization); B.B. (Conceptualization, methodology, formal analysis, investigation, data curation, writing—original draft preparation, writing-reviewing and editing, visualization); Y.P (Conceptualization, methodology, formal analysis, investigation, data curation, writing—original draft preparation, writing-reviewing and editing, visualization, supervision, project administration, funding acquisition). All authors have read and agreed to the published version of the manuscript.

Conflict of interest statement

The authors declare that they have no known competing financial interests or personal relationships that could have appeared to influence the work reported in this paper.

Funding

Micropore Technologies Ltd. and the University of Strathclyde 'Healthcare Nanotechnologies' Strathclyde Centre for Doctoral Training supported this work.

Institutional review board statement

All animals were handled in accordance with the UK Home Office Animals Scientific Procedures Act of 1986 in accordance with an internal ethics board and a UK government-approved project licence (Project licence PP1650440; Granted: 29 May 2020).

Data availability

The supplementary material is available online at https://doi.org/10.15129/23e3812f-01f9-41f7-9492-56c79d9f20c1

References

1. Webb C, Ip S, Bathula NV *et al*. Current status and future perspectives on MRNA drug manufacturing. *Mol Pharm* 2022;**4**:1047–58.
2. Shepherd SJ, Issadore D, Mitchell MJ. Microfluidic formulation of nanoparticles for biomedical applications. *Biomaterials* 2021;**274**:120826. https://doi.org/10.1016/j.biomaterials.2021.120826
3. Zhang NN, Li X-F, Deng Y-Q *et al*. A thermostable mRNA vaccine against COVID-19. *Cell* 2020;**182**:1271–83.e16. https://doi.org/10.1016/j.cell.2020.07.024
4. Buschmann MD, Carrasco MJ, Alishetty S *et al*. Nanomaterial delivery systems for mRNA vaccines. *Vaccines (Basel)* 2021;**9**:65. https://doi.org/10.3390/vaccines9010065
5. Webb C, Forbes N, Roces CB *et al*. Using microfluidics for scalable manufacturing of nanomedicines from bench to GMP: a case study using protein-loaded liposomes. *Int J Pharm* 2020;**582**:119266. https://doi.org/10.1016/j.ijpharm.2020.119266
6. Krzysztoń R, Salem B, Lee DJ *et al*. Microfluidic self-assembly of folate-targeted monomolecular siRNA-lipid nanoparticles. *Nanoscale* 2017;**9**:7442–53. https://doi.org/10.1039/c7nr01593c
7. Leung AK *et al*. Lipid nanoparticles containing siRNA synthesized by microfluidic mixing exhibit an electron-dense nanostructured core. *J Phys Chem C Nanomater Interfaces* 2012;**34**:18440–50.
8. Roces CB, Lou G, Jain N *et al*. Manufacturing considerations for the development of lipid nanoparticles using microfluidics.

Pharmaceutics 2020;**12**:1095. https://doi.org/10.3390/pharmaceutics12111095
9. Nakamura K, Aihara K, Ishida T. Importance of process parameters influencing the mean diameters of siRNA-containing lipid nanoparticles (LNPs) on the in vitro activity of prepared LNPs. *Biol Pharm Bull* 2022;**45**:497–507. https://doi.org/10.1248/bpb.b21-01016
10. Rabiee N, Dokmeci MR, Zarrabi A *et al*. Green Biomaterials: fundamental principles. *Green Biomaterials* 2023;**1**:1–4. https://doi.org/10.1080/29934168.2023.2268943
11. Pellegrino J, Schulte LR, De la Cruz J *et al*. Membrane processes in nanoparticle production. *J Membr Sci* 2017;**522**:245–56. https://doi.org/10.1016/j.memsci.2016.09.018
12. Piacentini E, RUsso B, Bazzarelli F *et al*. Membrane nanoprecipitation: From basics to technology development. *J Membr Sci* 2022;120564.
13. Laouini A, Charcosset C, Fessi H *et al*. Preparation of liposomes: a novel application of microengineered membranes–from laboratory scale to large scale. *Colloids Surf B* 2013;**112**:272–8. https://doi.org/10.1016/j.colsurfb.2013.07.066
14. Othman R, Vladisavljević GT, Nagy ZK *et al*. Encapsulation and controlled release of rapamycin from polycaprolactone nanoparticles prepared by membrane micromixing combined with antisolvent precipitation. *Langmuir* 2016;**32**:10685–93. https://doi.org/10.1021/acs.langmuir.6b03178
15. Chen GG, Luo GS, Xu JH *et al*. Membrane dispersion precipitation method to prepare nanoparticals. *Powder Technol* 2004;**139**:180–5. https://doi.org/10.1016/j.powtec.2003.12.003
16. Syed UT, Leonardo I, Lahoz R *et al*. Microengineered membranes for sustainable production of hydrophobic deep eutectic solvent-based nanoemulsions by membrane emulsification for enhanced antimicrobial activity. *ACS Sustain Chem Eng* 2020;**8**:16526–36. https://doi.org/10.1021/acssuschemeng.0c05612
17. Holdich R, Dragosavac M, Williams B *et al*. High throughput membrane emulsification using a single-pass annular flow cross-flow membrane. *AIChE J* 2020;**66**:e16958.
18. Vladisavljevic GT, Laouini A, Charcosset C *et al*. Production of liposomes using microengineered membrane and co-flow microfluidic device. *Colloids and Surfaces A: Physicochemical and Engineering Aspects*. 2014;**458**:168–77.
19. Zhang L, More KR, Ojha A *et al*. Effect of mRNA–LNP components of two globally-marketed COVID-19 vaccines on efficacy and stability. *NPJ Vaccines* 2023;**8**:156.
20. Di J, Du Z, Wu K *et al*. Biodistribution and non-linear gene expression of mRNA LNPs affected by delivery route and particle size. *Pharm Res* 2022;**39**:105–14. https://doi.org/10.1007/s11095-022-03166-5
21. Augustine, R., Hasan, A., Primavera, R *et al*. Cellular uptake and retention of nanoparticles: Insights on particle properties and interaction with cellular components. *Mater Today Commun* 2020;**25**:101692.
22. Forbes N, Hussain MT, Briuglia ML *et al*. Rapid and scale-independent microfluidic manufacture of liposomes entrapping protein incorporating in-line purification and at-line size monitoring. *Int J Pharm* 2019;**556**:68–81. https://doi.org/10.1016/j.ijpharm.2018.11.060
23. Webb C, Khadke S, Tandrup Schmidt S *et al*. The impact of solvent selection: strategies to guide the manufacturing of liposomes using microfluidics. *Pharmaceutics* 2019;**11**:653. https://doi.org/10.3390/pharmaceutics11120653
24. Jahn A, Vreeland WN, Gaitan M *et al*. Controlled vesicle self-assembly in microfluidic channels with hydrodynamic focusing. *J Am Chem Soc* 2004;**126**:2674–5. https://doi.org/10.1021/ja0318030
25. Maeki M, Fujishima Y, Sato Y *et al*. Understanding the formation mechanism of lipid nanoparticles in microfluidic devices with chaotic micromixers. *PLoS One* 2017;**12**:e0187962. https://doi.org/10.1371/journal.pone.0187962
26. Blakney AK, McKay PF, Yus BI *et al*. Inside out: optimization of lipid nanoparticle formulations for exterior complexation and in vivo delivery of saRNA. *Gene Ther* 2019;**26**:363–72. https://doi.org/10.1038/s41434-019-0095-2
27. Ly HH, Daniel S, Soriano SKV *et al*. Optimization of lipid nanoparticles for saRNA expression and cellular activation using a design-of-experiment approach. *Mol Pharm* 2022;**19**:1892–905. https://doi.org/10.1021/acs.molpharmaceut.2c00032
28. Meng N, Grimm D. Membrane-destabilizing ionizable phospholipids: novel components for organ-selective mRNA delivery and CRISPR–Cas gene editing. *Signal Transduct Target Ther* 2021;**6**:206. https://doi.org/10.1038/s41392-021-00642-z